



An extended hardness limit in bulk nanoceramics

James A. Wollmershauser^{*}, Boris N. Feigelson^{*}, Edward P. Gorzkowski, Chase T. Ellis, Ramasis Goswami, Syed B. Qadri, Joseph G. Tischler, Fritz J. Kub, Richard K. Everett

Naval Research Laboratory, 4555 Overlook Ave SW, Washington, DC 20375, USA

Received 3 December 2013; received in revised form 19 January 2014; accepted 19 January 2014

Abstract

Mechanical strengthening by grain refinement is a method whereby a material's strength and hardness can be increased by decreasing the average crystallite grain size. The empirical Hall–Petch relationship mathematically describes grain boundary strengthening and provides guidance for a straightforward way to produce stronger materials. While the phenomenon has been widely explored in nanocrystalline metals, the difficulty associated with fabricating high-quality dense nanocrystalline ceramics has left unanswered the question of the validity and extent of the relationship in ceramics. Prior studies suggest the occurrence of an inverse Hall–Petch response in ceramics with grain sizes <100 nm. This paper demonstrates a novel integrated approach, comprised of nanopowder processing and high-pressure, low-temperature sintering to fabricate bulk, fully dense and high-purity nanocrystalline ceramics with unprecedentedly small nanometer-sized grains. Using magnesium aluminate spinel as an archetypal hard ceramic, the hardness of this transparent ceramic armor is shown to rigorously follow the Hall–Petch relationship down to grain sizes of 28 nm. Consequentially, the nanocrystalline spinel ceramics are shown to exhibit a 50% increase in hardness over a corresponding order of magnitude reduction in grain size without a decline in density or fracture resistance. Additionally, the produced nanocrystalline ceramics have an optical transparency near theoretical. Reaching an exceptional hardness of 20.2 GPa at 28 nm, the behavior shows no evidence supporting an inverse Hall–Petch effect.

Published by Elsevier Ltd. on behalf of Acta Materialia Inc.

Keywords: Hall–Petch; Spinel; High-pressure sintering; Nanoceramic; Nanocrystalline ceramic

1. Introduction

Bulk materials consisting of nanostructures often exhibit unique and exciting mechanical properties, in many cases as a result of complex phenomena related to an unconventionally high ratio of atoms on interfaces, or grain boundaries, to atoms in the grain interior. However, bulk ceramic nanostructures in dense forms are extremely difficult to fabricate. Therefore, their basic properties, such as the dependence of mechanical properties on grain size, are difficult to elucidate. The empirical Hall–Petch relationship

describes the phenomenon whereby a material's strength and hardness can be increased by decreasing the average crystallite grain size [1,2]. The relationship provides guidance for a straightforward way to produce stronger and harder materials—potentially to the nanocrystalline level. Observation [3] and theory [4] explain that grain boundaries impede dislocation slip, the principal deformation mechanism accommodating strain during plasticity, and smaller grains limit dislocation pile-up sizes which affect how easily dislocations can traverse grain boundaries and travel from grain to grain. A higher applied stress is then necessary to propagate dislocations from grain to grain and permanently deform a material, effectively increasing yield strength [5] and hardness [6]. The limitations of the phenomenon have been widely scrutinized in metals and

^{*} Corresponding authors. Tel.: +1 202 767 5799 (J.A. Wollmershauser). Tel.: +1 202 767 0827 (B.N. Feigelson).

E-mail addresses: james.wollmershauser@nrl.navy.mil (J.A. Wollmershauser), boris.feigelson@nrl.navy.mil (B.N. Feigelson).

transitions to diffusion-based strain accommodation have been identified in nanocrystalline metals [4]. However, the validity of the slip-based Hall–Petch relationship in bulk and fully dense (i.e. pore free) nanocrystalline ceramics has not thoroughly been explored and, as a corollary, the understanding of the mechanical behaviors of nanocrystalline ceramics (specifically, hardness) is still not complete [7].

Fig. 1 summarizes literature hardness values for selected oxide ceramics [8–16] with various grain sizes, and reveals that for coarse, sub-micron and “ultra-fine” grain sizes, hardness follows a traditional Hall–Petch relationship, $H_v = H_0 + k/\sqrt{D}$, where H_v is the measured hardness, H_0 is the intrinsic hardness dependent on frictional lattice resistance to dislocation motion, k is the material-specific strengthening coefficient, and D is the average grain size. Importantly, these data also allude to the fact that very few studies explore the hardness of single-phase nanocrystalline oxide ceramics where grain sizes are <100 nm. The few existing studies exploring hardness of nanocrystalline ceramics demonstrate a deviation from a traditional Hall–Petch relationship and find decreasing hardness below ~130 nm in nanostructured MgO ceramics [8] (see Fig. 1) or no grain size dependence on hardening at all below 100–400 nm in TiO₂ [17,18]. Numerous studies on single-phase metallic systems [4] have defined decreasing hardness with decreasing grain size as an intrinsic response classified as an inverse Hall–Petch effect. However, the discrepancy in behavior of ceramics [8,17,18] suggests that the response is not underpinned by the same mechanism.

The shortage of published works on oxide ceramics with truly nanometer-scale grain sizes is largely a result of the

difficulty in producing bulk and fully dense ceramics that retain such small average grain sizes [7]. Sintering is the most versatile and successful fabrication method to produce ceramics from powders and, importantly, includes diffusion-based processes of densification and coarsening. Numerous variations on sintering exist, such as the use of microwave [19] or Joule [20] heating, and recent understanding has enhanced control [21–24], but retaining the nanoscale of powders with crystallite sizes smaller than ~50 nm in ceramics that are bulk and fully dense remains a challenge. Notably, the success of densification is strongly related to the quality of the powder, including morphology, purity and size distribution and the ideal powder structure is difficult to elucidate. In general, literature claims suggest that fine-grained powders improve sintering activity down to a limiting particle size, which often ranges between 200 and 100 nm [25]. Transitioning to finer nanoscale particles is expected to deteriorate sintering performance [26–28].

High-pressure sintering of nanopowders at low to moderate temperatures provides a potential avenue to fabricate bulk ceramics which retain nanostructures without dramatic grain growth [29]. This approach utilizes high pressures to break agglomerates and retard bulk diffusion rates while simultaneously exploiting the increased surface potential of nanoparticles for surface-energy-driven densification without coarsening. Interestingly, such an approach has been applied to MgAl₂O₄ spinel ceramics [30] but the nanocrystalline ceramics produced contained significant porosity (up to 3%) [31], leading to the conclusion that a simple combination of high pressures and elevated temperatures does not promote complete densification during sintering. More recent work [32] highlights that pre-treatment of nanopowders in high-temperature vacuum and argon environments promotes diffusion-based cohesion mechanisms at room temperature at high pressures, suggesting that powder processing and sintering environments, such as that developed in the present paper, play a critical role in the balance of densification and coarsening during high-pressure sintering.

This work explores the Hall–Petch relationship in oxide ceramics fabricated via high-pressure, low-temperature sintering of treated non-agglomerated nanoscale (21.1–33.6 nm) and submicron (200 nm) MgAl₂O₄ spinel powders. Fully dense nanocrystalline ceramics with grain sizes ranging from 28 to 53 nm are produced from the nanopowders. As part of the novel integrated approach, all powders for high-pressure processing are dried/calcined and remain in an inert, moisture-free environment throughout the subsequent processing. Mechanical and microstructural characteristics of the bulk dense nanocrystalline ceramics are investigated as a means to determine the degree of sintering and characterize the properties of the bulk dense nanocrystalline ceramics. Spinel is used as a transparent armor; therefore, optical transparency is as critical as mechanical hardness from a functional perspective. Transparent armors require porosity <0.01% [10]

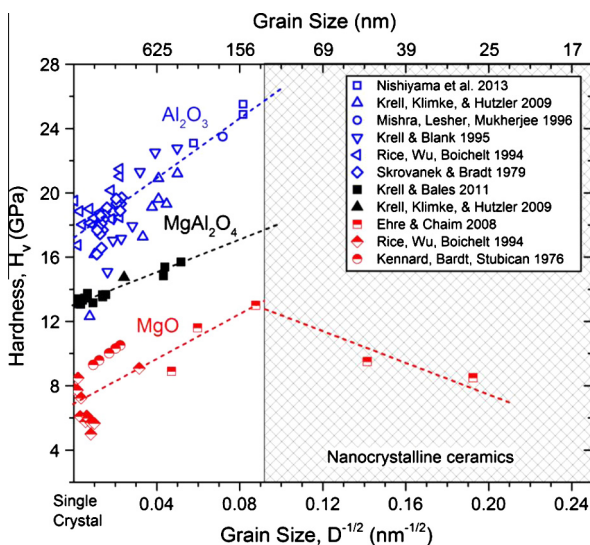


Fig. 1. Prior understanding of the grain size–hardness, i.e. Hall–Petch, relationship in ceramics including data from Refs. [8–16]. A Hall–Petch relationship follows a linear response when plotted in terms of $D^{-1/2}$. Limitations in fabrication of truly nanocrystalline ceramics have restricted exploration to bulk ceramics with grain sizes no lower than ~150 nm. A few studies exist in the nanometer range, including from Ref. [8] for MgO, and have shown an inverse Hall–Petch effect.

(densities >99.99% theoretical) and, in such materials, high inline transmission serves as a secondary verification of high density (which is also measured via the Archimedes principle). Vickers hardness is correlated with the grain sizes measured by X-ray diffraction and compared to literature values to ascertain the extent of a single-mechanism Hall–Petch relationship. Fractures resistance (i.e. toughness) estimates are also derived from the hardness indents.

2. Experimental

Several batches of high-purity non-agglomerated MgAl_2O_4 spinel nanopowders were obtained from Nanocer, Inc. (Ann Arbor, MI) with manufacturer-reported Brunauer–Emmett–Teller (BET) surface areas of 30, 35, 42, and $50 \text{ m}^2 \text{ g}^{-1}$. Impurity contents were listed in Ref. [32]. The powder particles are largely spherical and the particle size distribution is at least bimodal with the majority of particles in the 10 nm size regime and a few particles in the 100 nm regime [33]. To compare rgw sintering performance of different particle size regimes, submicron powder was obtained from Baikowski with a reported BET specific surface area of $30 \text{ m}^2 \text{ g}^{-1}$ and an average particle diameter of $0.2 \mu\text{m}$ [34]. Major impurities of the submicron powder are listed by the manufacturer as Fe at 10 ppm, Na at 10 ppm, Si at 20 ppm and Ca at 5 ppm.

Care was taken to reprocess the commercial powders to purify them without significant coarsening and keep them in a purified environment throughout the entire processing procedure to ensure a pristine surface during sintering. All powders were dried and calcined in a flowing oxygen environment in a quartz container at temperatures $>600 \text{ }^\circ\text{C}$. Processed powders were then transferred to a dry nitrogen glovebox ($<0.1 \text{ ppm O}_2$ and moisture) without exposure to air.

The powders were pressed into green compacts without binder within the glovebox in an evacuable die using 1900 kg cm^{-2} sample pressure. The ejected green compacts were 2–4 mm tall with a diameter of 11 mm. In each run, one, two or three green compacts were mechanically sealed in a metal capsule. The sealed sample capsule was inserted into the high-pressure assembly, which consists of a

partially sintered ZrO_2 container saturated with CsCl in the shape of a rectangular cuboid with truncated edges, a graphite heater, mica and molybdenum heater contacts. See Fig. 2 for a schematic. K-type thermocouples were inserted through both high-pressure cell assembly lids. A pressed boron nitride tablet isolated the exposed thermocouple junction from the metal sample capsule. The high-pressure experiments were performed in a press-less split-sphere apparatus (BARS) equipped with an 8–6 type multi-anvil system [35,36]. After a ~ 25 min pressurization to 2 GPa, samples were sintered at various temperatures from 740 to $845 \text{ }^\circ\text{C}$ (see Table 1 for exact processing temperature) for 15 min. A temperature deviation of $\sim 2 \text{ }^\circ\text{C}$ between the two thermocouples was typical. The cell assembly was cooled to room temperature before a 40 min pressure release to ambient pressure. Samples were cut from the high-pressure cell assembly after processing. Coarse-grit SiC paper was used to expose both sample surfaces. Progressively finer grit papers, up to 1200 grit, were used to smooth the sample surface. Both sides of the sample were polished with a $1 \mu\text{m}$ diamond suspension and washed with ethanol.

All characterization was done on the polished ceramics. Grain size was determined using a Halder–Wagner crystallite [37] size analysis of the integral peak width of X-ray diffraction data collected on a Rigaku X-ray powder diffractometer with $\text{Cu K}\alpha$ radiation from an 18 kW rotating anode source. Density was measured with an AccuPyc II 1340 pycnometer, via the Archimedes principle using He gas displacement and mass measurements. The nickel ring was not included in the density measurement. Inline absolute transmission (scattered light was not focused back to the detector) was measured over a wavelength of 200–3000 nm using a Perkin Elmer UV–Vis–NIR spectrophotometer (Lambda 750). Theoretical real inline transmittance (RIT) was estimated by the Apetz and Bryggen approach [38], which accounts for grain size effects $<1 \mu\text{m}$ and for the physical parameters of the specimens, $RIT = (1 - R_s) \exp\left(-\frac{3\pi^2 r \Delta n^2 d}{\lambda^2}\right)$ where R_s denotes the reflection losses at the surfaces and depends on the refractive index $n = 1.715$ [39], r is the grain size, $\Delta n = 0.005$ [40] is

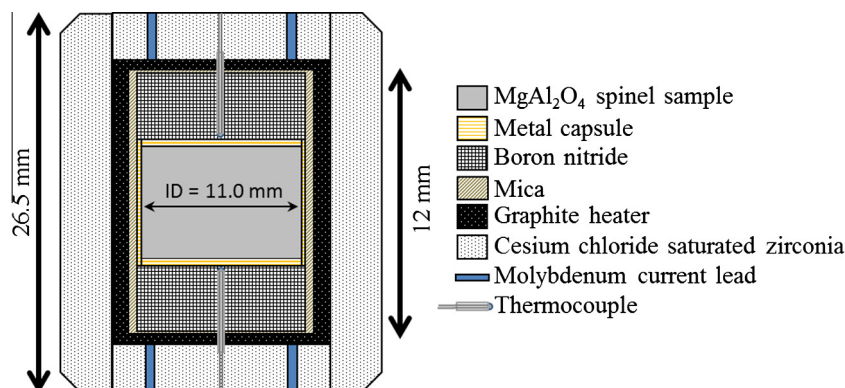


Fig. 2. Schematic of the high-pressure cell assembly.

Table 1
Powder size and grain size of treated commercial powders and nanocrystalline ceramics determined by XRD Halder–Wagner analysis. High-pressure processing temperature and pressure parameters are listed.

Average powder particle size (nm)	Processing pressure (GPa)	Processing temperature (°C)	Dense ceramic grain size (nm)
25.8	2	740	28
21.1	2	845	29.3
25.8	2	795	30.8
22.5	2	845	31.5
33.6	2	845	52.3
~200 ¹	2	795	>200 ²

¹ As reported by supplier. Average grain sizes larger than ~50 nm cannot be determined by XRD.

² Sintered ceramic not fully dense and grain size not characterized.

the discontinuity in the refractive index n at the grain boundaries, d is the sample thickness, and λ is the wavelength of the incident beam. R_s is estimated as $2R'/(1+R')$, where $R' = ((n-1)/(n+1))^2$. The microstructures of the ceramics were evaluated without a conductive metallic coating using a JEOL JSM-7001FLV scanning electron microscope operating in low-vacuum mode with N₂ gas for charge compensation. For TEM analysis, a spinel ceramic was crushed using a mortar and pestle in an alcohol medium. A few drops of alcohol containing fine powder were transferred onto a carbon-coated fine-mesh Cu grid. Micro-indentation hardness tests were performed with a Buehler Micromet II digital microhardness tester with a Vickers tip, 200 gf load and dwell time of 15 s. The reported Vickers hardness value for each nanocrystalline sample is the mathematical average of five indents taken from five different locations. An estimate of fracture toughness is determined by $K = \frac{0.0726P}{c^2}$ [41], where P is the load and c is crack length from the center of the indent. All indents produced only four visible surface cracks emanating from each corner of

the Vickers indent. Toughnesses were determined from the average crack lengths of between four and eight indents. It is noted that the Vickers indentation fracture (VIF) technique used in this study is not equivalent to a standardized fracture toughness test, and therefore the two toughness values cannot be directly compared. Consequently, measured toughness values are compared only to toughness values reported using the same VIF technique and the experimentally measured parameter is referred to here as a fracture resistance.

3. Results and discussion

3.1. Microstructure of nanocrystalline spinel ceramics

Analysis of the X-ray diffraction peak locations and widths demonstrates that the ceramics fabricated by high-pressure sintering are single phase and nanocrystalline. The diffraction pattern presented in Fig. 3a is collected from a nanocrystalline ceramic sintered at 2 GPa and 795 °C. The diffraction peaks correspond to stoichiometric magnesium aluminate [42] and a nickel ring that holds the sample (see Fig. 3b). The average grain size of the ceramic in Fig. 3 is 30.8 nm, while the crystallite size of the powder was initially 25.8 nm, indicating that minimal coarsening had occurred. Table 1 lists the average crystallite size of the powders and ceramics as well as the processing conditions. Although various initial powder sizes and sintering temperatures are utilized in the study, very little coarsening occurs during sintering at 2 GPa and moderate temperatures, i.e. <40% of the melting temperature. The measured density of the nanocrystalline ceramic characterized in Fig. 3 is found to be $3.6005 \pm 0.0079 \text{ g cm}^{-3}$, which is equal to that of stoichiometric magnesium aluminate [43] and reveals that the produced ceramics are fully dense.

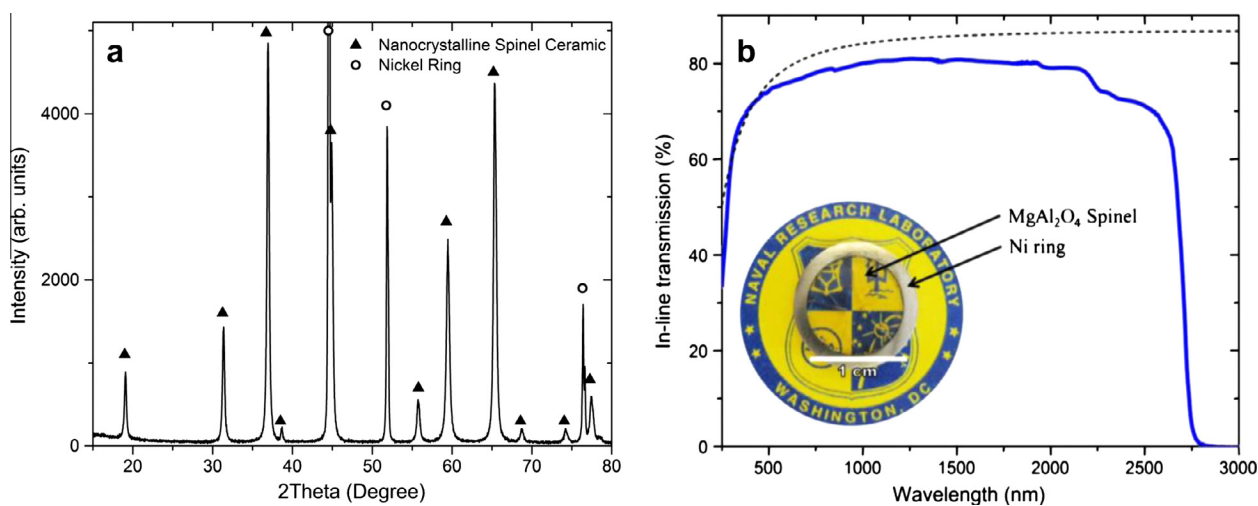


Fig. 3. (a) X-ray diffraction pattern showing presence of spinel phase and nickel peaks that correspond to a nickel ring that holds the sample (shown in (b)). Halder–Wagner analysis of the integral peak widths shows that the grain size of the ceramic is 30.8 nm. (b) In-line optical transmission (solid line) of high-pressure sintered nanocrystalline spinel with grain size 30.8 nm (same sample as in (a)) and thickness of 1.6 mm compared to theoretical real in-line transmission (dashed line). Inset: photograph of 30.8 nm spinel ceramic in front of the NRL logo. A nickel ring holds the sample.

While simple visual inspection, such as that shown in the inset of Fig. 3b, establishes that the nanocrystalline ceramics are transparent in the visible spectrum, the inline transmission spectra in Fig. 3b reveals that the nanocrystalline ceramics are transparent without major absorption bands from ultraviolet to short-infrared wavelengths. The maximum measured transmission reaches $\sim 81\%$ at infrared wavelengths of 1200–1350 nm. Since the cubic spinel structure produces no birefringence [44], optical scattering is only influenced by second phases with a refraction index different from that of the matrix and is not influenced by the additional boundaries and interfaces introduced via a reduced grain size. The experimental transmission is compared to the theoretical RIT, shown in Fig. 3b (dashed line). The deviation from theoretical transmission is small and further preparation of the surfaces for optical clarity (e.g. improving parallelism of surfaces and surface roughness) should increase the transmission to near the mathematical theoretical limit [38].

As a more technologically relevant comparison, spinel ceramics with micron and submicron grain sizes produced by a variety of methods explored in Ref. [25] exhibit maximum transmissions ranging from 81 to 84% over similar wavelengths. Therefore, the optical quality of the presently produced nanocrystalline spinel ceramics is consistent with industry standards for microcrystalline and submicrocrystalline ceramics. Additionally, the inset in Fig. 3b reveals that the nanocrystalline spinel ceramics are colorless, an industry criterion for spinel windows. Other spinel ceramics produced by high-pressure processing have been produced with a light brown color [30], suggesting that the powder processing and sintering environment adopted

presently either does not introduce or removes sufficient contaminants from the nanopowder to protect their purity during consolidation. The high optical quality of the nanocrystalline ceramics also serves to verify a high density since pores contribute to optical scattering and degrade transparency [45]. The high levels of transparency demonstrated presently and in Ref. [25] result from extremely low residual porosities which are required for transparent armor [10].

The micrographs in Figs. 4 and 5 further support that the ceramics are fully dense while also revealing that high-pressure sintering at low temperatures excels at densifying nanopowders and produces high-quality ceramics without residual porosity or marked grain growth. Fig. 4a and b compare SEM micrographs of the polished surface of a ceramic sintered from 200 nm powder and the same 30.8 nm nanocrystalline ceramic presented in Fig. 3. The samples were sintered in the same sample capsule at 2 GPa and 795 °C to eliminate variability in the sintering environment. Fine, distributed porosity is present in the micrograph of the submicron sample (Fig. 4a), while very few features, which include a surface scratch and dust particles, are present at similar magnification for the nanocrystalline ceramic (Fig. 4b). At higher magnifications, a submicron grain structure is apparent in the coarse ceramic and abnormally large grains decorate the porous structure. TEM, shown in Figs. 4d and 5, is required to view the grain structure of the nanocrystalline ceramics. Fig. 4d clearly shows a nanocrystalline grain structure.

Comparison of the microstructures in Fig. 4 reveals that, contrary to prior reports [25–28], reducing powder particle size down to tens of nanometers does not

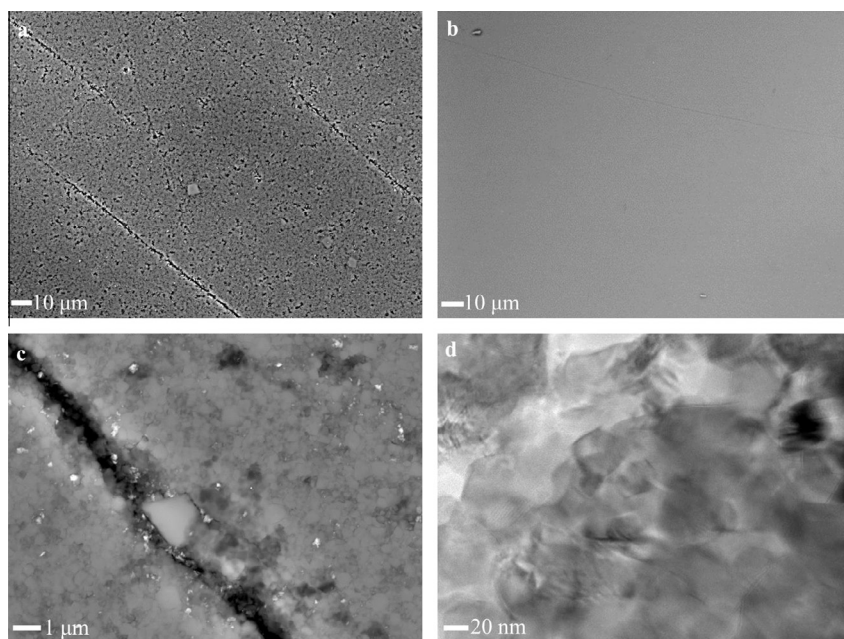


Fig. 4. Microstructure of porous and fully dense spinel ceramics produced by sintering at 2 GPa and 795 °C. (a and c) SEM micrographs of the porous submicron structure of spinel ceramic sintered from 200 nm sized spinel powder. (b) SEM and (d) TEM images show the fully dense microstructure of the same nanocrystalline ceramic present in Fig. 2 sintered from 25.8 nm powder.

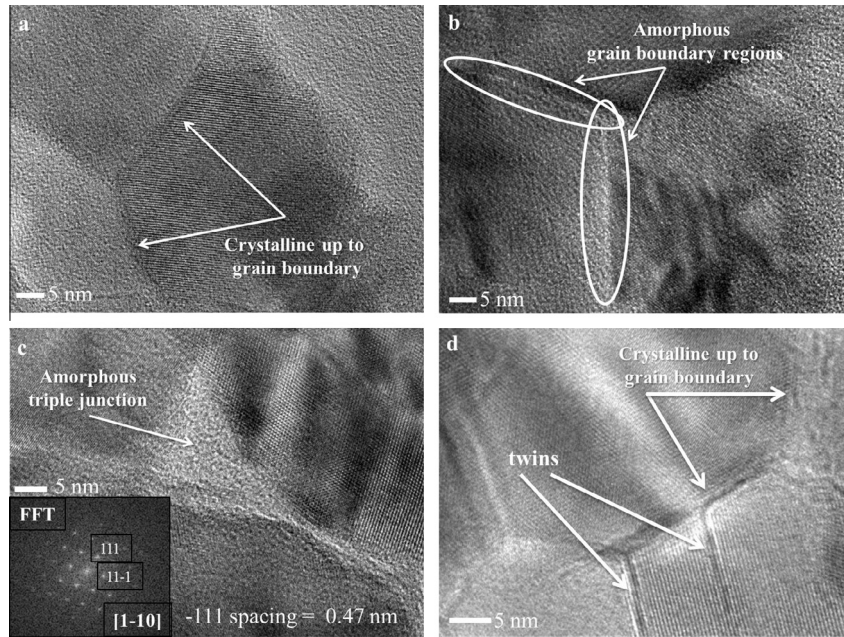


Fig. 5. Transmission electron spectroscopy of fully dense ceramics produced by sintering at 2 GPa and 795 °C. (a) and (b) Present different areas and reveal that some grain boundaries contain ~ 1 nm amorphous phase regions. (c) Shows an amorphous triple junction and the inset shows the fast Fourier transform of the main figure. The diffraction pattern is from the $[1-10]$ orientation and indicates that the -111 spacing is 0.47 nm. (d) Micrograph from a region containing nanotwins.

necessarily impede sintering activity of ceramics at high pressures, and, advantageously, can allow sintering at low homologous temperatures. The combination of high pressure, nanosized particles and low temperature allows the production of nanocrystalline ceramics without dramatic grain growth.

Further scrutiny of the microstructure of the sintered nanoceramics reveals several interesting features. Fig. 5 presents TEM micrographs of different grain boundary regions and shows nanoscale grains where the crystalline lattice extends up to the boundary (Fig. 5a,d), as well as other boundaries decorated with a small, ~ 1 nm, amorphous phase region (Fig. 5b) characterized by a lighter contrast. An amorphous phase can also be seen at the junction of three grains in Fig. 4c. Bulk optical and density measurements reveal that the fabricated nanocrystalline ceramics are fully dense and highly transparent; therefore, the material is characterized as containing a small volume percentage of amorphous grain boundaries that has a negligible influence on its optical properties and density. Additionally, it will be subsequently shown that the amorphous content and the presence of twins (see Fig. 5d) also have a negligible influence on the measured mechanical response. The 111 lattice spacing, calculated from Fig. 5c, equals 0.814 nm ($\pm 1\%$) which is consistent with standards [42].

3.2. Hardness and the Hall–Petch relationship in hard spinel ceramics

Hardness measurements reveal that a traditional dislocation-based Hall–Petch relationship is valid in hard

Table 2

Hardness and fracture resistance determined from Vickers indentation. Error is tabulated as standard error.

Dense ceramic grain size (nm)	Vickers hardness (GPa)	Fracture resistance ($\text{MPa m}^{1/2}$)
28	20.2 ± 0.54	1.99 ± 0.01
29.3	19.38 ± 0.16	2.02 ± 0.04
30.8	18.9 ± 0.34	*
31.5	19.23 ± 0.38	2.04 ± 0.02
52.3	17.93 ± 0.07	1.98 ± 0.11
$>200^2$	¹	¹

¹ Sintered ceramic not fully dense and mechanical properties not characterized.

² Sintered ceramic not fully dense and grain size not characterized.

* Sample used for TEM study before toughness determinations.

ceramics down to at least 28 nm, resulting in an unprecedented hardness of 20.2 GPa in magnesium aluminate spinel ceramics. Table 2 lists the measured hardness of each nanocrystalline ceramic produced in the present study by high-pressure processing. Fig. 6 plots the hardness of the nanocrystalline spinel ceramics and the literature hardness values for spinel ceramics produced by a variety of other methods [10,12] that have conventional, submicron and ultrafine grain sizes as a function of grain size. The observed single linear relation follows the mathematical Hall–Petch expression $H_v = H_0 + k/\sqrt{D}$, where H_0 and k are determined by regression to be 13.39 and 33.42, respectively. The complete set of hardness data does not reveal a change in hardening response or a maximum hardness, such as that observed in simple metals [4] or in prior

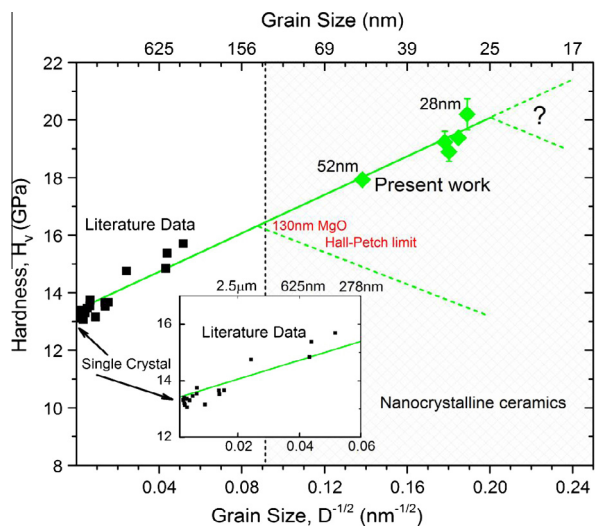


Fig. 6. Hall–Petch plot comparing Vickers hardness and grain size for magnesium aluminate spinel ceramics. See Fig. 1 for references of square data points. Diamond data points from the present work and from various nanocrystalline spinel ceramics formed by high-pressure processing. A single linear dependence describes the hardening relationship for all spinel ceramics down to 28 nm. This is compared to Fig. 1 where data from prior studies on MgO ceramics identified a Hall–Petch limit near 130 nm.

ceramic studies [8,17,18], which previously resulted in the classification of an inverse Hall–Petch effect.

The presence of a single linear relationship suggests that the established strain accommodation mechanism active in spinel ceramics, identified as $\langle 110 \rangle$ slip [46], is the dominant mechanism in nanocrystalline ceramics. It can therefore be inferred that diffusion-based mechanisms, such as grain boundary slip and grain rotation, are not dominating the room-temperature deformation in these nanocrystalline ceramics. Since twins are characterized in the microstructure (see Fig. 5d), their potential influence on the mechanical response should also be considered. Twins can act as additional barriers to dislocations, effectively decreasing the apparent grain size, and increase hardness. However, the single linear dependence of hardness on the average grain size suggests that twins do not play a strong role in the hardening response of strain accommodation in nanocrystalline spinel ceramics.

Fracture resistance estimates of the nanocrystalline ceramics range from 1.98 to 2.04 MPa $m^{1/2}$ (see Table 2). Importantly, the fracture resistances measured for the nanocrystalline ceramics falls within the range determined for polycrystalline spinel ceramics, 1.19–2.21 MPa $m^{1/2}$ [47]. The lack of a grain size dependence on fracture resistance suggests that the fracture mode is the same in ceramics with nanometer- and micrometer-sized grains.

The present work shows the validity of the Hall–Petch relationship in spinel ceramics down to 28 nm and reveals that prior grain size–hardness responses suggesting an inverse Hall–Petch effect in nanocrystalline ceramics are likely the result of microstructural features other than grain size. Indeed, the MgO and TiO₂ ceramics characterized in Refs. [8,17,18] contained up to 6.4% porosity. Based on

the current work, high-pressure sintering of spinel and other oxide nanopowders with initial particle sizes < 10 nm may be possible and provide an avenue to fabricate the necessary bulk ceramics to investigate the upper limit of hardness and strength in ceramics.

4. Conclusions

The Hall–Petch relationship has been proven in fully dense magnesium aluminate spinel ceramics down to 28 nm grain sizes, and, as a result, a unique hardness of 20.2 GPa for spinel ceramics has been demonstrated for the first time. The single linear dependence supports the hypothesis that a single dislocation-based mechanism, principally $\langle 110 \rangle$ slip, is accommodating strain in spinel ceramics within all grain size regimes explored in the present work and presented in the literature. The high-pressure sintering employed in the present work shows that the sintering activity in nanometer spinel/oxide powders is not necessarily impeded and provides an avenue to fabricate and explore the mechanical behavior of ceramics and other fully dense materials with single-digit nanometer grain sizes. The discovery of unconventionally high hardness in nanocrystalline spinel ceramics demonstrates the suitability of this approach for the development of new super-hard and ultra-hard nanoceramic materials.

Acknowledgements

The authors gratefully acknowledge the Naval Research Laboratory basic research program and Office of Naval Research for support of this work. J.A.W. acknowledges the NRL Karles Fellowship for support. C.T.E. acknowledges support from the National Research Council. J.A.W., B.N.F., and F.J.K. acknowledge support from Dr. Lawrence T. Kabacoff.

References

- [1] Hall EO. Proc Phys Soc B 1951;64:747.
- [2] Petch NJ. J Iron Steel Inst 1953;174:25–8.
- [3] Whelan MJ, Hirsch PB, Horne RW. Proc R Soc London A 1957;240:524–38.
- [4] Meyers MA, Mishra A, Benson DJ. Prog Mater Sci 2006;51:427–556.
- [5] Dieter GE. Mechanical metallurgy. 3rd ed. New York: McGraw-Hill; 1961.
- [6] Hall EO. Nature 1954;173:948–9.
- [7] Maglia F, Tredici IG, Anselmi-Tamburini U. J Euro Ceram Soc 2013;33:1045–66.
- [8] Ehre D, Chaim R. J Mater Sci 2008;43:6139–43.
- [9] Kennard FL, Bradt RC, Stubican VS. J Am Ceram Soc 1976;59:160–3.
- [10] Krell A, Bales A. Int J Appl Ceram Technol 2011;8:1108–14.
- [11] Krell A, Blank P. J Am Ceram Soc 1995;78:1118–20.
- [12] Krell A, Klimke J, Hutzler T. J Euro Ceram Soc 2009;29:275–81.
- [13] Mishra RS, Leshner CE, Mukherjee AK. J Am Ceram Soc 1996;79:2989–92.
- [14] Nishiyama N et al. Scripta Mater 2013;69:362–5.
- [15] Rice RW, Wu CC, Boichelt F. J Am Ceram Soc 1994;77:2539–53.

- [16] Skrovanek SD, Bradt RC. *J Am Ceram Soc* 1979;62:215–6.
- [17] Averbach RS, Höfler HJ, Hahn H, Logas JC. *Nano Mater* 1992;1:173–8.
- [18] Edelstein AS, Cammaratra RC. *Nanomaterials: synthesis, properties and applications*. 2nd ed. New York: CRC Press; 1998. p. 616.
- [19] Roy R, Agrawal D, Cheng J, Gedevisanishvili S. *Nature* 1999;399:668–70.
- [20] Omori M. *Mater Sci Eng A* 2000;287:183–8.
- [21] Binner J, Vaidhyanathan B. *J Euro Ceram Soc* 2008;28:1329–39.
- [22] Chaim R, Levin M, Shlayer A, Estournes C. *Adv App Ceram* 2008;107:159–69.
- [23] Holland TB et al. *J Euro Ceram Soc* 2012;32:3667–74.
- [24] Oghbaei M, Mirzaee O. *J Alloys Compd* 2010;494:175–89.
- [25] Krell A, Hutzler T, Klimke J, Potthoff A. *J Am Ceram Soc* 2010;93:2656–66.
- [26] Cook R, Kochis M, Reimanis I, Kleebe H-J. *Proc SPIE* 2005;5786:41–7.
- [27] Li G, Jiang A, Zhang L. *J Mater Sci Lett* 1996;15:1713–5.
- [28] Li JG, Sun X. *Acta Mater* 2000;48:3103–12.
- [29] Groza JR, Dowding RJ. *Nano Mater* 1996;7:749–68.
- [30] Lu TC et al. *Appl Phys Lett* 2006;88:213120.
- [31] Lu T, Chang X, Zhang J, Qi J, Luo X. *Key Eng Mater* 2008;368–372:402–6.
- [32] Wollmershauser JA et al. *Scripta Mater* 2013;69:334–7.
- [33] Nanocerox, Inc., Ann Arbor, MI. Spinel MgAl₂O₄, Powder characteristics; 2013. <http://www.nanocerox.com/product_spinel.htm>.
- [34] Baikowski. France; 2013. <<http://www.baikowski.com/products.php?s=3&ss=&p=43>>.
- [35] Charles SJ et al. *Phys Stat Sol A* 2004;201:2473–85.
- [36] Vins VG, Feigelson BN, Yelissev AP. *Soviet J Superhard Mater* 1991;3:21.
- [37] Halder NC, Wagner CNJ. *Acta Crystall* 1966;20:312.
- [38] Apetz R, van Bruggen MPB. *J Am Ceram Soc* 2003;86:480–6.
- [39] Frage N, Cohen S, Meir S, Kalabukhov S, Dariel MP. *J Mater Sci* 2007;42:3273–5.
- [40] Rothman A, Kalabukhov S, Sverdlov N, Dariel MP, Frage N. *Int J Appl Ceram Technol* 2012;1–8.
- [41] Evans AG, Charles EA. *J Am Ceram Soc* 1976;59:371–2.
- [42] Wang CC, McFarlane III SH. *J Cryst Growth* 1968;3–4:485–9.
- [43] Lee M. PhD thesis. University of Colorado at Boulder Biomedical Engineering, Boulder; 2007.
- [44] Krell A, Hutzler T, Klimke J. *Ceram For Int* 2007;84:50–6.
- [45] Goldstein A. *J Euro Ceram Soc* 2012;32:2869–86.
- [46] Mitchell TE. *J Am Ceram Soc* 1999;82:3305–16.
- [47] Dericoglu AF, Boccaccini AR, Dlouhy I, Kagawa Y. *Mater Trans* 2005;46:996–1003.